Dynamics of interstitial skyrmions in the presence of temperature gradients

Lingyao Kong [1], Xianliang Chen,[1] Weiwei Wang [2,3,*] Dongsheng Song,[2] and Haifeng Du[4]

[1]*School of Physics and Materials Science, Anhui University, Hefei 230601, China*
[2]*Institutes of Physical Science and Information Technology, Anhui University, Hefei 230601, China*
[3]*Key Laboratory of Structure and Functional Regulation of Hybrid Materials of Ministry of Education, Anhui University, Hefei 230601, China*
[4]*Anhui Key Laboratory of Condensed Matter Physics at Extreme Conditions, High Magnetic Field Laboratory, HFIPS, Anhui, Chinese Academy of Sciences, Hefei 230031, China*

An interstitial skyrmion is the skyrmion state confined in the helical background. While the spin helix naturally provides the one-dimensional channels in helical magnets, the dynamics of an interstitial skyrmion are different from that for free skyrmions in a ferromagnetic or conical background. In this paper, we studied the dynamics of interstitial skyrmions under a temperature gradient numerically and analytically. We show that the interstitial skyrmion moves from the hot area to the cold area in the presence of temperature gradients, in contrast to skyrmions in the ferromagnetic background, where they move towards the hot region. Because the interstitial skyrmion is confined in the one-dimensional channel, it moves in the same direction as the magnon flow induced by the temperature gradient, where the β-type thermomagnonic torque plays an essential role.

Magnetic skyrmions are topological spin textures that have a quantized topological number [1,2] and particlelike properties [3]. The latter enable the skyrmions to be considered as promising candidates for spintronic applications, such as logic devices [4], racetrack memory [5,6], and neuromorphic computation [7]. One effective mechanism to stabilize the magnetic skyrmions is the Dzyaloshinskii-Moriya interaction (DMI) [8–10], which supports the helical states naturally with a weak external field. Interestingly, the skyrmion also can exist in the helical background, forming an interstitial skyrmion [11]. Compared with the skyrmion in the ferromagnetic background, the interstitial skyrmion has its features. For example, the one-dimensional channels are naturally provided by the helical background, which may result in a fast skyrmion motion [12]. Moreover, the interstitial skyrmion chain can be formed with attractive interactions due to the repulsive forces provided by the surrounding helical phase [11].

Magnetic skyrmions show fascinating dynamics in nonequilibrium environments. For example, ratchet skyrmion motion emerges in the presence of temperature gradients where the skyrmions are confined in a round disk [13]. Theoretical studies show that the skyrmion will move towards the high-temperature region [14,15] in the presence of temperature gradients, which is different from the typical particle diffusion. This prediction is observed experimentally in an insulating magnet using Lorentz transmission electron microscopy [16]. Meanwhile, skyrmions moving to the cold region were observed in multilayer systems [17], implying subtle skyrmion dynamics in the nonequilibrium environments [18]. It is interesting to ask which region the interstitial skyrmion will move towards in the presence of temperature gradients.

In this paper, we investigate the dynamics of interstitial skyrmions in the presence of temperature gradients numerically and analytically. We show that interstitial skyrmions move towards the cold area, which is contrary to the skyrmion motion in the ferromagnetic background [14,15].

We consider a classical Heisenberg model on a regular cubic lattice with nearest-neighbor exchange interaction, the bulk-type DMI, and a weak uniaxial anisotropy. Accordingly, the system's Hamiltonian can be written as

$$\mathcal{H} = -J \sum_{\langle i,j \rangle} \mathbf{m}_i \cdot \mathbf{m}_j + \sum_{\langle i,j \rangle} \mathbf{D}_{ij} \cdot [\mathbf{m}_i \times \mathbf{m}_j]$$
$$- \sum_i K(\mathbf{e}_x \cdot \mathbf{m}_i)^2, \tag{1}$$

where $\langle i, j \rangle$ represents a unique pair of lattice sites i and j and $\mathbf{m}_i$ is the unit vector of the magnetic moment $\boldsymbol{\mu}_i = -\hbar\gamma\mathbf{S}_i$ with $\mathbf{S}_i$ being the atomic spin and $\gamma(>0)$ being the gyromagnetic ratio. The bulk-type DMI vector $\mathbf{D}_{ij}$ can be written as $\mathbf{D}_{ij} = D\hat{\mathbf{r}}_{ij}$, where D is the DMI constant and $\hat{\mathbf{r}}_{ij}$ is the unit vector between $\mathbf{S}_i$ and $\mathbf{S}_j$. In this paper, we have used $D/J = 0.36$ and $K/J = 0.009$ to speed up the calculation. We have ignored the external field, which is not essential for stabilizing the helical structures and interstitial skyrmions.

A system of size $N = 600 \times 220 \times 4$ sites with open boundary conditions is selected to study the dynamics of the interstitial skyrmion. The micromagnetic package JU-MAG [19], which is graphics processor unit (GPU) supported, was used to perform the simulation. Moreover, we have chosen $J = \hbar = \gamma = k_B = S = a = 1$ as simulation parameters [13,20], and thus the coefficients to convert the time t, temperature T, and velocity v to SI units are $\hat{t} = \hbar S/J$,

_____
*wangweiwei@ahu.edu.cn

TABLE I. Unit conversion table for $J = 50$ K, $S = 1/2$, and $a = 0.5$ nm.

	Conversion	Value
Distance x	$\hat{x} = a$	$= 0.5$ nm
Time t	$\hat{t} = \hbar S/J$	≈ 76.4 fs
Velocity v	$\hat{v} = Ja/(hS)$	$\approx 1.04 \times 10^3$ m/s
Temperature T	$\hat{T} = J/k_B$	$= 50$ K

$\hat{T} = J/k_B$, and $\hat{v} = Ja/\hbar S$, respectively. For typical insulating Cu_2OSeO_3, $J = 50$ K, $S = 1/2$, we take the lattice spacing $a = 0.5$ nm, and the corresponding coefficients are shown in conversion units in Table I. An interstitial skyrmion in the helical background is shown in Figs. 1(a) and 1(b), which is obtained by minimizing the system energy. Figure 1(a) shows an interstitial skyrmion in the helical background, which is obtained by minimizing the system energy. Compared with the skyrmion in the ferromagnetic background in which the external field is used to stabilize the isolated skyrmion, the interstitial skyrmion is stabilized by the helix surrounding it. Therefore a skyrmion chain can also be formed, as shown in Fig. 1(c), where the chain contains three individual skyrmions.

The dynamics of the magnetic moment in a nonzero-temperature environment is governed by the Landau-Lifshitz-Gilbert (LLG) equation with a stochastic field **h**:

$$\frac{\partial \mathbf{m}_i}{\partial t} = -\gamma \mathbf{m}_i \times (\mathbf{H}_{\text{eff}} + \mathbf{h}_i) + \alpha \mathbf{m}_i \times \frac{\partial \mathbf{m}_i}{\partial t}, \quad (2)$$

where $\mathbf{H}_{\text{eff}} = -(1/\mu_s)\partial\mathcal{H}/\partial\mathbf{m}_i$ is the total effective field and α is the Gilbert damping. The thermal fluctuation is assumed to be a Gaussian white noise; that is, the thermal noise obeys the properties [21,22]

$$\langle \mathbf{h}_i \rangle = 0, \quad \langle \mathbf{h}_i^u(t), \mathbf{h}_j^v(t') \rangle = 2D_0 \delta_{ij}\delta_{uv}\delta(t-t'), \quad (3)$$

where i and j are Cartesian indices, u and v indicate the field components, and the average $\langle \cdots \rangle$ is taken over different realizations of the stochastic field. The strength of the thermal fluctuations is determined by $D_0 = (\alpha k_B T)/(\gamma \mu_s) = (\alpha k_B T)/(\hbar\gamma^2 S)$. Although the magnitude of classical spin S influences the strength of thermal fluctuation fields, it has no impact on the conversion relation $\hat{T}$, as shown in Table I.

We first study the Brownian motion of the interstitial skyrmions. In the presence of a uniform temperature, the thermal fluctuation field immediately has two effects. The
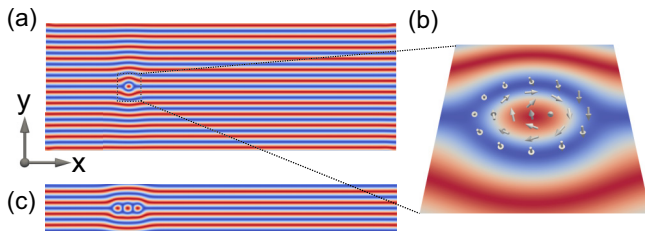

FIG. 1. (a) The studied system is a simple cubic lattice with a size of $600 \times 220 \times 4$ in which an interstitial skyrmion is immersed in the helical background. (b) A zoom-in plot of the interstitial skyrmion is shown in (a). (c) A skyrmion chain is composed of three interstitial skyrmions.
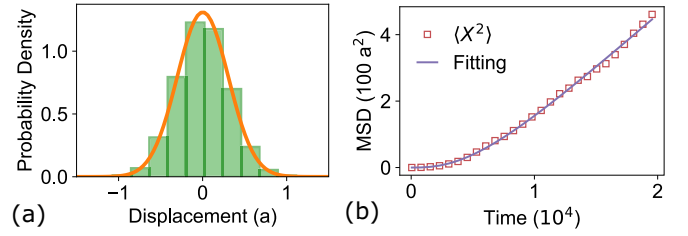

FIG. 2. (a) Histogram of the X displacements within $\Delta t = 25$ for the interstitial skyrmion at temperature $T = 0.02$. A Gaussian fit (shown as an orange line) is performed with the fitted $\sigma = 1.24a$. (b) The mean-square displacement (MSD) as a function of the elapsed time, where 32 trajectories with length $N = 800$ and $\Delta t = 25$ are used. The Gilbert damping is set to be $\alpha = 0.01$.

fluctuation field breaks the static standard skyrmion profile, leading to an effective skyrmion mass. The established typical skyrmion mass is of the order of 1×10^{-25} kg [22,23]. Meanwhile, the skyrmion performs a random walk which can be seen by measuring its geometric center (X, Y). Figure 2(a) shows a histogram of the displacements of X within $\Delta t = 25$ at temperature $T = 0.02$. The distribution of the displacements can be well described using a Gaussian function, indicating that the skyrmion feels a white noise "force" collectively. The mean-square displacement (MSD) of the skyrmion position, defined as $\langle X^2 \rangle(t) = \langle |X(t) - X_0|^2 \rangle$, is plotted in Fig. 2(b). Compared with the skyrmion in the ferromagnetic background, the interstitial skyrmion is confined in the one-dimensional channel, and thus the skyrmion can only move freely in the x direction, which agrees with the calculated MSDs. $\langle X^2 \rangle$ scales with time linearly, and $\langle Y^2 \rangle$ reaches a constant in the long-time limit.

To understand the dynamics of interstitial skyrmion, we use the approach developed by Thiele [24] and consider the translational motion $\mathbf{m}(\mathbf{r}, t) = \mathbf{m}[\mathbf{r} - \mathbf{R}(t)]$, i.e., ignoring the skyrmion mass. We obtain

$$G\mathbf{e}_z \times \mathbf{v}_d + \alpha\mathcal{D} \cdot \mathbf{v}_d = \mathbf{f} - \nabla U, \quad (4)$$

where $\mathbf{v}_d$ is the skyrmion velocity. The z-component gyrovector $G = 4\pi Q$, and $Q = \int_\Omega \mathbf{m} \cdot (\partial_x \mathbf{m} \times \partial_y \mathbf{m})dxdy = \pm 1$ is the skyrmion number where the integral is taken over the skyrmion area Ω. For the interstitial skyrmion shown in Fig. 1(b), the skyrmion area can be determined using the contour line with $m_z = -1$ since the spin in the skyrmion's core is pointed up ($m_z = 1$). The tensor $\mathcal{D}$ represents the shape factor of spin textures and is given by $\mathcal{D}_{ij} = \int_\Omega (\partial_i \mathbf{m} \cdot \partial_j \mathbf{m}) \, dx \, dy$. The $\mathcal{D}$ can be simplified as $\mathcal{D}_{ij} = \delta_{ij}D$ when the spin textures have the rotational symmetry and $D \sim 4\pi$ for a magnetic skyrmion. The collective stochastic force $\mathbf{f}_i = -\gamma \int_\Omega (\partial_i \mathbf{m} \cdot \mathbf{h})dxdy$, and therefore its average over the ensemble reads $\langle f_i(t+\tau)f_j(t) \rangle = (2\alpha D' k_B T/\mu_s)\delta_{ij}\delta(\tau)$. The potential $U = U(Y)$ is introduced phenomenologically, which represents the pushing force imposed by the helical background. By using the quadratic approximation for the potential $U = U(Y) = (\kappa/2)Y^2$, we arrive at

$$dX = a\, dW_1 + b\, dW_2 - c_1 Y dt, \quad (5)$$

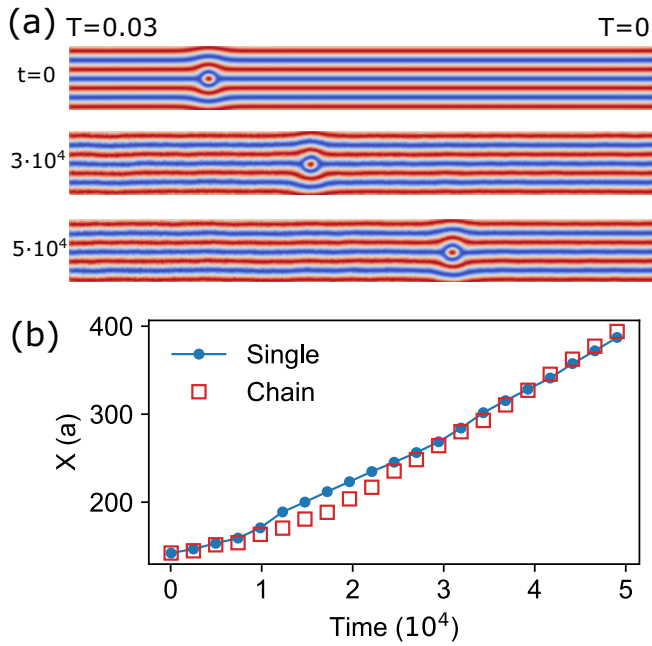$$dY = -b\, dW_1 + a\, dW_2 - c_2 Y dt, \quad (6)$$

FIG. 3. (a) Snapshots of an interstitial skyrmion at time $t = 0$, 3×10^4, and 5×10^4 in the presence of a temperature gradient $dT/dx = -5 \times 10^{-5}$, where the Gilbert damping $\alpha = 0.008$ is used. (b) The time-dependent positions of the interstitial skyrmion and a chain with three interstitial skyrmions. Both the interstitial skyrmion and skyrmion chain move towards the cold region.

where W_1 and W_2 represent two Wiener processes, $a = \alpha D\eta/(\alpha^2 D^2 + G^2)$, $b = G\eta/(\alpha^2 D^2 + G^2)$, $c_1 = \kappa G/(\alpha^2 D^2 + G^2)$, $c_2 = \alpha\kappa D/(\alpha^2 D^2 + G^2)$, and $\eta = \sqrt{2\alpha D' k_B T/\mu_s}$. The average $\langle X \rangle$ and $\langle Y \rangle$ can be calculated by solving $d\langle X \rangle/dt = -c_1\langle Y \rangle$ and $d\langle Y \rangle/dt = -c_2\langle Y \rangle$, which gives $\langle X \rangle = 0$ and $\langle Y \rangle = 0$ for initial conditions $X_0 = 0$ and $Y_0 = 0$. Similarly, the average of X^2 and Y^2 can be evaluated using

$$d\langle X^2 \rangle/dt = -2c_1\langle XY \rangle, \tag{7a}$$

$$d\langle XY \rangle/dt = -c_1\langle Y^2 \rangle - c_2\langle XY \rangle, \tag{7b}$$

$$d\langle Y^2 \rangle/dt = \eta^2 - 2c_2\langle Y^2 \rangle, \tag{7c}$$

which results in

$$\langle X^2 \rangle = \left(\eta^2 c_1^2/2c_2^3\right)(2c_2 t + 4e^{-c_2 t} - e^{-2c_2 t} - 3) \tag{8}$$

and $\langle Y^2 \rangle = (\eta^2/2c_2)(1 - e^{-2c_2 t})$. The simulation results of $\langle X^2 \rangle$ are fitted using Eq. (8), and the fitted parameters are $c_2 = 2.65 \times 10^{-4}$ and $\eta^2 c_1^2/c_2^2 = 0.032$. In the long-time limit, we obtain

$$\langle X^2 \rangle = \frac{2G^2 D' k_B T}{\alpha D^2} t \tag{9}$$

and $\langle Y^2 \rangle = 2(\alpha^2 D^2 + G^2)k_B T/\kappa$. The expression (9) shows that the diffusion coefficient is inversely proportional to the Gilbert damping, which is different from the case of a skyrmion in the ferromagnetic background [15].

The simulation results in the presence of a temperature gradient are shown in Fig. 3. The temperature of the left end of the sample is set to 0.03, while the right side is as-

sumed to be 0 K, and thus the constant temperature gradient is $dT/dx = -5 \times 10^{-5}$. Figure 3(a) shows snapshots of the interstitial skyrmion at time $t = 0$, 3×10^4, and 5×10^4. The interstitial skyrmion moves along the $+x$ direction, i.e., moves toward the cold region. This phenomenon is different from the theoretical prediction for the skyrmion dynamics in the ferromagnetic background, where the skyrmions move towards the hot area [14]. The corresponding skyrmion position as a function of time is illustrated in Fig. 3(b). As a comparison, the position for a skyrmion chain containing three skyrmions is also plotted. The skyrmion velocity increases in the first stage ($\sim 3 \times 10^4$), and after that, a steady motion with the established average velocity $\sim 5.7 \times 10^{-3}$ is observed.

The presence of temperature gradients has two effects on the dynamics of interstitial skyrmions. The first is that the Brownian diffusion will result in a net skyrmion motion. Note that the characteristic relations [Eqs. (7a)–(7c)] between $\langle X^2 \rangle$, $\langle XY \rangle$, and $\langle Y^2 \rangle$ are the same as those for the standard Langevin equation of the Brownian particle, where Y plays the role of velocity and κ is the effective mass. Therefore the average net velocity due to the Brownian diffusion is [25,26]

$$\langle v_B \rangle = -\frac{G^2 D' k_B}{\alpha D^2}\frac{dT}{dx}. \tag{10}$$

The minus sign shows that the skyrmion moves towards the colder area under the Brownian diffusion.

The second contribution is that the temperature gradients break the equilibrium state of thermal magnons. Thus thermal magnons propagate from the hot region to the cold region, forming a spin-wave spin current [27,28]. When the thermal magnons pass through the skyrmion, magnons transfer angular momentum to the skyrmion and result in the skyrmion motion. To illustrate the interplay between the spin currents and the skyrmion, we split the unit vector $\mathbf{m}$ into two orthogonal components [29,30]: $\mathbf{m} = \sqrt{1 - \delta\mathbf{m}^2}\,\mathbf{m}_0 + \delta\mathbf{m}$, where the slow component $\mathbf{m}_0$ represents the equilibrium profile of the spin textures and the fast component $\delta\mathbf{m}$ denotes the small deviation from $\mathbf{m}_0$ owing to the thermal fluctuations. Inserting it back into the LLG equation, and averaging over the quadratic terms in the fast component $\delta\mathbf{m}$, one obtains the total thermomagnonic torque [30]

$$\boldsymbol{\tau} = \hbar(\mathbf{J} \cdot \nabla)\mathbf{m}_0 - (\hbar A/s)\partial_i\rho(\mathbf{m}_0 \times \partial_i\mathbf{m}_0), \tag{11}$$

where $J_i = (A/\hbar)[\mathbf{m}_0 \cdot (\delta\mathbf{m} \times \partial_i\delta\mathbf{m})]$ is the magnon flux density, $A = J/(2a)$ is the exchange constant, and $\rho = s\langle\delta\mathbf{m}^2\rangle/(2\hbar)$ is the magnon number density with $s = \hbar S/a^3$ being the spin angular-momentum density [30]. The first term on the right-hand side of Eq. (11), originating from the longitudinal component of the spin current (defined as $J_i^s = -A\langle\delta\mathbf{m} \times \partial_i\delta\mathbf{m}\rangle$), represents the angular-momentum transfer between magnons and spin textures. The second term, also known as β-type torque, results from the gradient of the magnon number density ρ [30]. The macroscopic variables $\mathbf{J}$ and ρ can be simply expressed as $\mathbf{J} = -c_J\nabla T$ and $\nabla\rho = c_\rho\nabla T$. In the exchange-magnon approximation, the coefficients of c_J and c_ρ can be established as [30]

$$c_J = \frac{I_d}{2^d \pi^{d/2}}\frac{k_B}{\alpha\hbar\lambda^{d-2}}, \quad c_\rho = \frac{d\,I_d}{2^{d+1}\pi^{d/2}}\frac{s k_B}{A\hbar\lambda^{d-2}}, \tag{12}$$

where $\lambda = \sqrt{\hbar A/(sk_B T)}$ is the thermal magnon wavelength, $I_d \equiv [1/\Gamma(1 + d/2)] \int_0^\infty d\eta \eta^{d/2} e^\eta (e^\eta - 1)^{-2}$ is a numerical constant, and for the three-dimensional case $I_3 \approx 2.612$. Note that the ratio of c_J and c_ρ links $\mathbf{J}$ and $\nabla\rho$, which gives $\nabla\rho = -\beta(s/A)\mathbf{J}$, where $\beta \equiv (A/s)c_\rho/c_J = (d/2)\alpha$.

Integrating the torque τ into the Thiele equation, we obtain

$$G\mathbf{e}_z \times (\hbar\mathbf{J} + \mathbf{v}_d) + \mathcal{D} \cdot (\alpha\mathbf{v}_d - \beta\hbar\mathbf{J}) = \mathbf{f} - \nabla U. \quad (13)$$

In the ferromagnetic background the skyrmion can move freely, i.e., the potential $U = 0$, the velocity for the steady skyrmion motion reads $v_x = -[(G^2 - D^2\alpha\beta)/(G^2 + \alpha^2 D^2)]\hbar J_x$ and $v_y = -[(\alpha + \beta)DG/(G^2 + \alpha^2 D^2)]\hbar J_x$. Since J_x represents the magnon flux density from the hot region to the cold region, the skyrmion will move towards the hot area owing to the thermomagnonic torques [14]. The skyrmion Hall effect thus is given by $\tan\theta_h \equiv v_y/v_x = (\alpha + \beta)DG/(G^2 - D^2\alpha\beta)$. For the case of interstitial skyrmions, the potential imposed by the helical background restricts the interstitial skyrmion motion in the x direction, i.e., the skyrmion Hall angle $\theta_h \approx 0$. Therefore the steady motion of the interstitial skyrmions is given by

$$v_x = \frac{\beta}{\alpha}\hbar J_x = -\frac{\hbar d c_J}{2}\frac{dT}{dx}. \quad (14)$$

The above equation clearly shows that the velocity of the interstitial skyrmion is parallel to J_x, i.e., the interstitial skyrmion moves towards the cold area, where the β-type torque plays an essential role in such a direction reverse.

It is worth mentioning that an alternative theory to describe the interaction between spin waves and the skyrmion is to consider it as a magnon-skyrmion scattering problem [31,32]. In the framework of the Thiele equation, the magnons impose an extra force on the skyrmion, where the force can be written as [32,33]

$$\mathbf{F} = k\sigma_\parallel \hbar\mathbf{J} - Qk\sigma_\perp \hbar(\mathbf{e}_z \times \mathbf{J}), \quad (15)$$

where $\sigma_\parallel = \sigma_\parallel(\epsilon)$ and $\sigma_\perp = \sigma_\perp(\epsilon)$ are longitudinal and transverse transport scattering cross sections of the skyrmion and ϵ is the spin-wave energy. It can be seen from Eq. (13) that the $\sigma_\parallel$ and $\sigma_\perp$ components of the force [Eq. (15)] correspond to the β-type torque and the spin-current torque in Eq. (11), respectively. The skyrmion Hall angle predicted by the force [Eq. (15)] is related to the ratio $\sigma_\parallel/\sigma_\perp$, which normally depends on the spin-wave energy. Especially, in the low-energy limit ($kr_s \ll 1$, where r_s is the skyrmion radius), $\sigma_\parallel/\sigma_\perp \to \infty$ and thus the skyrmion moves approximately perpendicularly to the magnon current direction. However, the skyrmion Hall angle predicted by the torque [Eq. (11)] does not depend on the spin-wave energy. Note that the excited thermal magnons have a wide frequency range, and thus we add a correction force $\mathbf{F}_\parallel$ in Eq. (13),

$$\mathbf{F}_\parallel = \nu\hbar\mathbf{J}, \quad (16)$$

where ν is a coefficient. This correction force contributes an extra velocity for the interstitial skyrmions
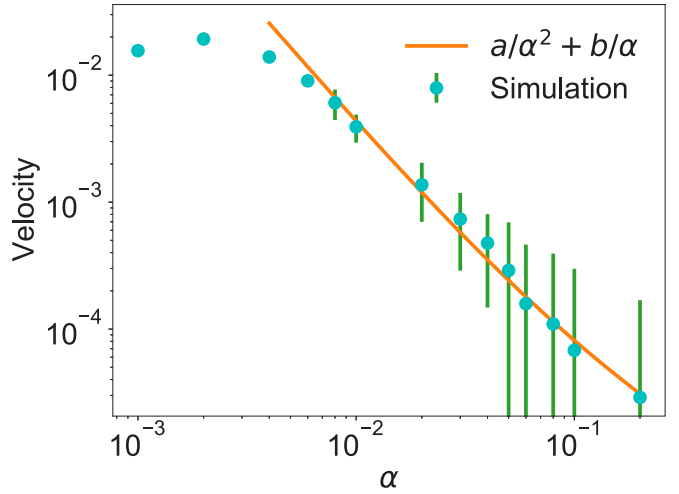
$$v_x' = \frac{\nu}{\alpha D}\hbar J_x. \quad (17)$$

FIG. 4. The average velocity of the interstitial skyrmion as a function of Gilbert damping α. Each data point is computed from ten trajectories, and the error bar represents the standard deviation of the ten velocities (20 trajectories are used for $\alpha \geqslant 0.02$). The damping-velocity relation is fitted using $v(\alpha) = a/\alpha^2 + b/\alpha$ with the fitted parameters $a = (3.9 \pm 0.4) \times 10^{-7}$ and $b = (4.2 \pm 0.9) \times 10^{-6}$.

Adding all three velocities [Eqs. (10), (14), and (17)] together, we obtain the overall velocity for interstitial skyrmions under a temperature gradient

$$\langle v_x \rangle = -\frac{\nu c_J'}{\alpha^2 D}\frac{dT}{dx} - \frac{dc_J'}{2\alpha}\frac{dT}{dx} - \frac{G^2 D' k_B}{\alpha D^2}\frac{dT}{dx}, \quad (18)$$

where $c_J' = I_d k_B/(2^d \pi^{d/2}\lambda^{d-2})$. Note that all terms have a minus sign, indicating similar contributions for thermal magnons and the Brownian motion—both drive the interstitial skyrmion from the hot region to the cold region. To check the validity of Eq. (18), we perform the numerical simulations with different Gilbert damping at a fixed temperature gradient $dT/dx = -5 \times 10^{-5}$. The average velocities are calculated, as shown in Fig. 4, in which the error bar is the standard deviation of ten velocities obtained from ten trajectories (20 trajectories are used for $\alpha \geqslant 0.02$). The damping-velocity relation for $\alpha \geqslant 0.006$ is fitted using the function $v(\alpha) = a/\alpha^2 + b/\alpha$, and the obtained fitting parameters $a = (3.9 \pm 0.4) \times 10^{-7}$ and $b = (4.2 \pm 0.9) \times 10^{-6}$. The coefficient ν can be established as $\nu = (a/b)(d/2)D \approx 1.2$. The last two terms on the right-hand side of Eq. (18) contribute to the fitting parameter b. So we have $-(dT/dx)c_J'd/2 \approx 1 \times 10^{-5}$ for the $d = 2$ case and $-(dT/dx)c_J'd/2 \approx 6 \times 10^{-7}$ for the $d = 3$ case where we simply assumed $I_2 \sim I_3$. Using the fitted parameter η and c_2, the contribution of the Brownian diffusion reads $-(dT/dx)G^2 D'/D^2 k_B = 4 \times 10^{-7}$. Our studied system is a quasi-two-dimensional system since it only has four layers in the z direction and the fitted parameter b is indeed bounded by the predictions for the $d = 2$ and $d = 3$ cases.

In summary, we have studied the dynamics of interstitial skyrmions in the presence of temperature gradients numerically and analytically. We show that the interstitial skyrmion moves from the hot region to the cold region in the pres-

ence of a temperature gradient, which is different from the case of a skyrmion in the ferromagnetic background. The thermomagnonic torques as well as the helical background, which imposes a pushing force to the interstitial skyrmion, play essential roles in the moving direction of the skyrmion.

[1] S. Mühlbauer, B. Binz, F. Jonietz, C. Pfleiderer, A. Rosch, A. Neubauer, R. Georgii, and P. Böni, Science **323**, 915 (2009).

[2] X. Z. Yu, Y. Onose, N. Kanazawa, J. H. Park, J. H. Han, Y. Matsui, N. Nagaosa, and Y. Tokura, Nature (London) **465**, 901 (2010).

[3] N. Nagaosa and Y. Tokura, Nat. Nanotechnol. **8**, 899 (2013).

[4] X. Zhang, M. Ezawa, and Y. Zhou, Sci. Rep. **5**, 9400 (2015).

[5] A. Fert, V. Cros, and J. Sampaio, Nat. Nanotechnol. **8**, 152 (2013).

[6] J. Tang, Y. Wu, W. Wang, L. Kong, B. Lv, W. Wei, J. Zang, M. Tian, and H. Du, Nat. Nanotechnol. **16**, 1086 (2021).

[7] K. M. Song, J.-S. Jeong, B. Pan, X. Zhang, J. Xia, S. Cha, T.-E. Park, K. Kim, S. Finizio, J. Raabe, J. Chang, Y. Zhou, W. Zhao, W. Kang, H. Ju, and S. Woo, Nat. Electron. **3**, 148 (2020).

[8] I. Dzyaloshinskii, J. Phys. Chem. Solids **4**, 241 (1958).

[9] T. Moriya, Phys. Rev. **120**, 91 (1960).

[10] W.-S. Wei, Rare Met. (Beijing) **40**, 3076 (2021).

[11] J. Müller, J. Rajeswari, P. Huang, Y. Murooka, H. M. Rønnow, F. Carbone, and A. Rosch, Phys. Rev. Lett. **119**, 137201 (2017).

[12] R. Knapman, D. R. Rodrigues, J. Masell, and K. Everschor-Sitte, J. Phys. D: Appl. Phys. **54**, 404003 (2021).

[13] M. Mochizuki, X. Z. Yu, S. Seki, N. Kanazawa, W. Koshibae, J. Zang, M. Mostovoy, Y. Tokura, and N. Nagaosa, Nat. Mater. **13**, 241 (2014).

[14] L. Kong and J. Zang, Phys. Rev. Lett. **111**, 067203 (2013).

[15] M. Weißenhofer, L. Rózsa, and U. Nowak, Phys. Rev. Lett. **127**, 047203 (2021).

[16] X. Yu, F. Kagawa, S. Seki, M. Kubota, J. Masell, F. S. Yasin, K. Nakajima, M. Nakamura, M. Kawasaki, N. Nagaosa, and Y. Tokura, Nat. Commun. **12**, 5079 (2021).

[17] Z. Wang, M. Guo, H.-A. Zhou, L. Zhao, T. Xu, R. Tomasello, H. Bai, Y. Dong, S.-G. Je, W. Chao, H.-S. Han, S. Lee, K.-S. Lee, Y. Yao, W. Han, C. Song, H. Wu, M. Carpentieri, G. Finocchio, M.-Y. Im *et al.*, Nat. Electron. **3**, 672 (2020).

[18] C. Gong, arXiv:2108.02621 [cond-mat].

[19] JUMAG-A JULIA package for classical spin dynamics and micromagnetic simulations with GPU support, https://github.com/ww1g11/JuMag.jl.

[20] W. Wang, M. Beg, B. Zhang, W. Kuch, and H. Fangohr, Phys. Rev. B **92**, 020403(R) (2015).

[21] X. S. Wang and X. R. Wang, Phys. Rev. B **90**, 014414 (2014).

[22] C. Schütte, J. Iwasaki, A. Rosch, and N. Nagaosa, Phys. Rev. B **90**, 174434 (2014).

[23] Y. Suzuki, S. Miki, Y. Imai, and E. Tamura, Phys. Lett. A **413**, 127603 (2021).

[24] A. A. Thiele, Phys. Rev. Lett. **30**, 230 (1973).

[25] D. Zubarev and A. Bashkirov, Physica (Amsterdam) **39**, 334 (1968).

[26] A. Pérez-Madrid, J. Rubí, and P. Mazur, Phys. A (Amsterdam) **212**, 231 (1994).

[27] U. Ritzmann, D. Hinzke, and U. Nowak, Phys. Rev. B **89**, 024409 (2014).

[28] S. R. Etesami, L. Chotorlishvili, A. Sukhov, and J. Berakdar, Phys. Rev. B **90**, 014410 (2014).

[29] A. A. Kovalev, Phys. Rev. B **89**, 241101(R) (2014).

[30] S. K. Kim and Y. Tserkovnyak, Phys. Rev. B **92**, 020410(R) (2015).

[31] C. Schütte and M. Garst, Phys. Rev. B **90**, 094423 (2014).

[32] S. Schroeter and M. Garst, Low Temp. Phys. **41**, 817 (2015).

[33] X. Zhang, J. Müller, J. Xia, M. Garst, X. Liu, and Y. Zhou, New J. Phys. **19**, 065001 (2017).